AJNR

Fast spin-echo MR of contact points on implanted intracerebral stainless steel multicontact electrodes.

L C Meiners, C J Bakker, P C van Rijen, C W van Veelen, A C van Huffelen, A van Dieren, G H Jansen and W P Mali

AJNR Am J Neuroradiol 1996, 17 (10) 1815-1819
http://www.ajnr.org/content/17/10/1815

Fast Spin-Echo MR of Contact Points on Implanted Intracerebral Stainless Steel Multicontact Electrodes

Linda C. Meiners, Chris J. G. Bakker, Peter C. van Rijen, Cees W. M. van Veelen, Alexander C. van Huffelen, Andre van Dieren, Gerard H. Jansen, and Willem P. T. M. Mali

Summary: A three-dimensional fast spin-echo MR technique is proposed for locating contact points on implanted intracerebral multicontact electrode bundles. Coronal or sagittal reformatting shows the entire trajectory of the electrode bundles. The contact points are clearly visible owing to the absence of coating material associated with a slightly larger susceptibility artifact. Potentially, this technique may preclude postimplantation thin-section CT, with its associated high radiation dose.

Index terms: Brain, magnetic resonance; Seizures

In preoperative examinations to locate seizure focus in patients with therapy-resistant epilepsy, it is sometimes necessary to implant subdural and intracerebral electrodes. Once the electrodes are placed, the position of the contact points must be verified. A variation on the method of combined implantation of intracerebral and subdural electrodes proposed by van Veelen et al (1) was used in the present study. This method consists of preimplantation three-dimensional magnetic resonance (MR)-guided stereotactic surgery with a Leksell frame and postimplantation 3-D computed tomographic (CT) examination as described by Gerritsen et al (2). Postimplantation CT is, however, associated with a high radiation dose, and the electrode contact points are not visible on CT scans. Large susceptibility artifacts associated with the commonly used 3-D gradient-echo MR volume imaging also limit visibility of the contact points. In an attempt to overcome these limitations, a postimplantation 3-D fast spin-echo MR sequence is proposed.

Materials and Methods

Patients

The MR images of three patients who were referred for surgical treatment of drug-resistant epilepsy were used in this study. Extensive preimplantation examinations included ictal and interictal surface electroencephalographic (EEG) recording with video monitoring, MR imaging, and positron emission tomography. Because these studies did not center on one abnormal area in the brain, evaluation with depth-electrode EEG registration was undertaken.

Materials

The depth electrodes consisted of six insulated recording wires glued around one supporting stainless steal wire (Brain Electronics, De Bilt, the Netherlands). The contact points on the intertwined recording wires were created by removing the polymer biocompatible coating over a short distance at different levels for each wire (Fig 1A–D). The four distal contact points were 2.5 mm long separated by 2.5-mm intervals. The remaining two proximal contacts were 5 mm in length separated by 7.5-mm intervals. The total diameter of a depth-electrode bundle was 0.4 mm. The depth electrodes and the method of implantation have been described in detail (1).

Before the patients were studied, the electrodes were tested for ferromagnetism. No deflection was found, which was in agreement with the findings described by Brooks et al (3). Our electrodes consisted of an alloy containing 14% chromium and 12% nickel. As this alloy is similar to that described in the study by Zhang et al (4), the heat produced during MR imaging was considered negligible.

Study Design

For each patient a preimplantation 3-D gradient-echo MR image was obtained on a 0.5-T system with an MR-compatible Leksell stereotactic frame (Electra, Stockholm, Sweden) in situ. Implantation of the depth elec-

Received November 16, 1995; accepted after revision February 15, 1996.

From the Departments of Radiology (L.C.M., C.J.G.B., W.P.T.M.M.), Neurosurgery (P.C.V.R., C.W.M.V.V.), Clinical Neurophysiology (A.C.V.H.), Surgery (A.V.D.), and Pathology (G.H.J.), University Hospital Utrecht (the Netherlands).

Address reprint requests to Linda C. Meiners, MD, Department of Radiology, University Hospital Utrecht, Heidelberglaan 100, 3584 CX Utrecht, the Netherlands.

AJNR 17:1815–1819, Nov 1996 0195-6108/96/1710–1815

Fig 1. *A*, Photograph of intracerebral electrode with two contact point lengths indicated by *arrowheads* (enlargement ×2, similar to that of *E* and *F*).

B, Schematic representation of electrode bundle with the six separate contact points indicated.

C, Microscopic view of the electrode bundle. The bare area of one electrode forming a contact point is well seen.

D, Microscopic view of radiograph of the electrode bundle at the same level as *C*. The radiolucent dots represent the coating. At the level of a contact point (*arrows*) the number of radiolucent dots is diminished owing to a tighter twist.

E, Coronal reformatted 3-D T1-weighted gradient-echo image (30/13 [repetition time/echo time], 30° flip angle) of the depth electrodes in a gelatin phantom.

F, Coronal reformatted 3-D T1-weighted fast spin-echo sequence (550/13) of the same phantom as in *E* shows a decrease of susceptibility artifacts as compared with the gradient-echo sequence *E*. A contact point coinciding with the point on the electrode indicated in *A* is shown (*arrow*).

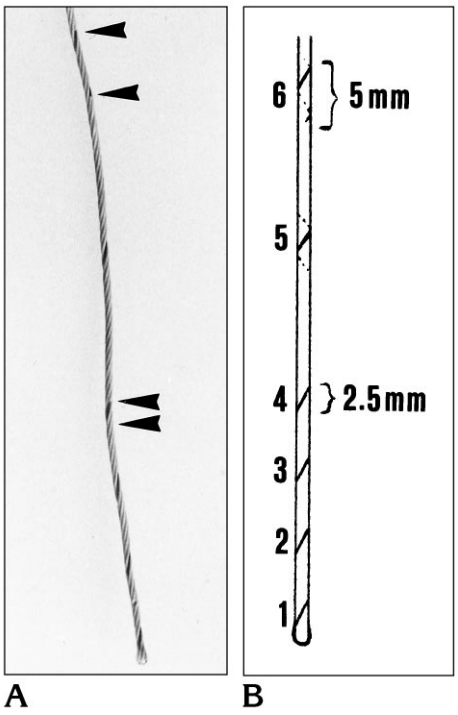

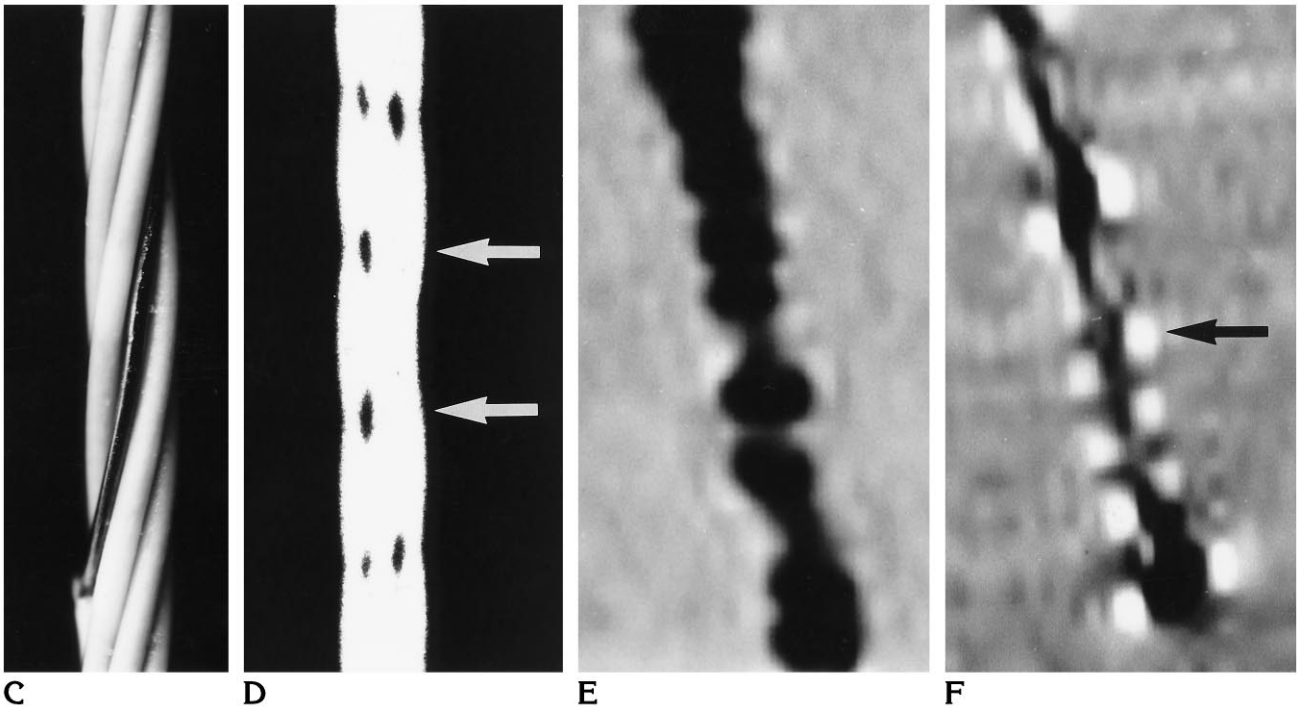

Three fast spin-echo sequences used in three patients with implanted depth electrodes

	Patient 1	Patient 2	Patient 3
Repetition time	550	550	550
Echo time	13	13	13
Field of view (FOV)	250	250	250
Rectangular FOV, %	80	80	80
Echo train length	5	5	5
Profile order*	Centric	Centric	Centric
No. of excitations	1	1	1
Scan, %	90	90	90
Bandwidth/pixel	166	197	166
Section thickness, mm	1.5	1.2	1.5
Overlapping sections	Yes	No	No
No. of sections	120	120	108
No. of volume chunks	10	10	6
Phase-encoding direction	Left-right	Left-right	Anteroposterior
Scan time, min	5.34	11.01	17.31

* First measurement is made at K_0 followed by profile acquisition in alternating fashion at progressively increasing distances from starting point.

trodes was performed via MR-guided stereotactic surgery. After the electrodes were placed, a 3-D reformatted CT scan was obtained with the stereotactic frame in place. This was done to exclude the possibility that an intracranial hematoma had developed and to determine the location of the implanted electrodes. When the preimplantation MR image was matched with the postimplantation CT scan, it was possible to depict the electrode bundles; however, the separate contact points were not visible.

An MR examination was performed 2 days after the implantation procedure and removal of the frame to determine the final position of the electrodes before EEG registration. A 3-D T1-weighted fast spin-echo sequence was used in all three cases, with an orientation similar to that of the preoperative MR study. The parameters used for the three patients were slightly modified in order to obtain an optimal scan sequence. The three sequences used are shown in the Table.

To demonstrate the advantage of fast spin-echo over gradient-echo for the postoperative MR examination, the depth electrodes were scanned in a phantom consisting of gelatin using the scanning sequences described above (Fig 1E and F).

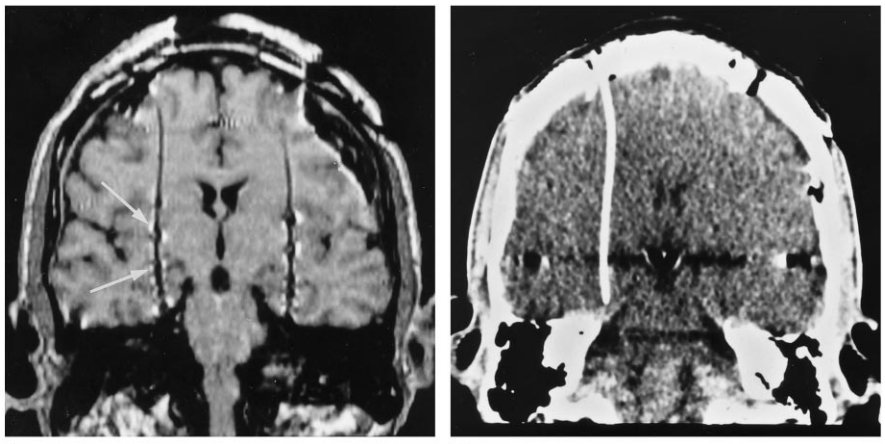

Fig 2. *A*, Coronal reformatted T1-weighted fast spin-echo MR image (550/13) shows the trajectory of the depth electrodes. The six contact points are well demarcated owing to a local increase in susceptibility artifacts (*arrows*).

B, Coronal reformatted CT scan shows the same trajectory of the electrode as seen on the MR image (*A*).

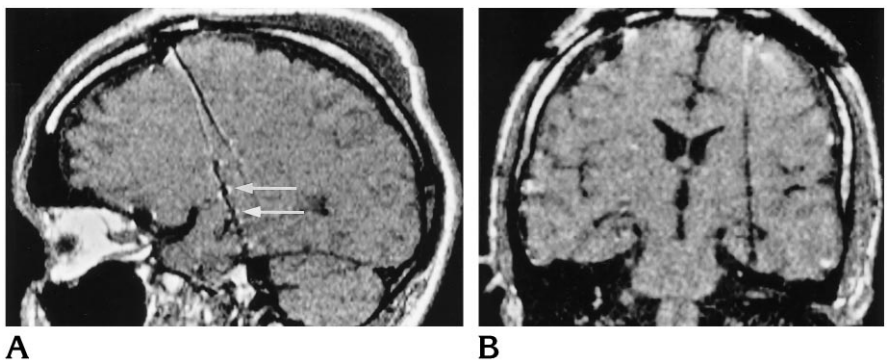

Fig 3. *A*, Sagittal reformatted fast spin-echo MR image (550/13), section thickness of 1.2 mm with left-to-right phase-encoding gradient, shows the separate contact points (*arrows*).

B, Coronal reformatted fast spin-echo MR image (550/13) with 1.2-mm section thickness and left-to-right phase-encoding direction. The contact points are less visible.

Results

The fast spin-echo images of the phantom study confirmed the reduction in metal artifacts accompanying the electrodes as compared with the gradient-echo sequence (Fig 1E and F).

The 3-D fast spin-echo acquisition allowed reformatting in multiple planes (Figs 2 and 3). Reformatting of the postimplantation axial images in the coronal and sagittal planes showed the trajectory of the intracerebral depth electrodes (Figs 2A and 3A), which was comparable to that shown on the postoperative CT scan (Fig 2A and B). The contact points created a small area of increased susceptibility artifacts. The position of the contact points on the MR images corresponded to the area in which the polymer biocompatible coating was removed, as shown in the phantom study in Figure 1. With the use of an anteroposterior phase-encoding gradient direction, the electrode contact points were best seen and isolated on the coronal reformatted images. A phase-encoding direction from left to right resulted in optimal depiction in the sagittal reformatted plane, with the susceptibility artifact projecting in the anteroposterior direction relating to the frequency-encoding gradient (Fig 3A). In the latter case, the individual contact points could not be isolated on the coronal reformatted images (Fig 3B).

Discussion

The development of 3-D MR imaging and later of appropriate computer programs adjusted to different stereotactic frames has made it possible to indicate accurately the desired intracerebral position of electrodes prior to surgery. Postimplantation CT with 1.5-mm sections followed by 3-D reformatting provides a method to determine the position of intracerebral and subdural stainless steel electrodes. Matching the preimplantation MR image with the postimplantation CT scan has proved to be a useful technique to depict the exact anatomic location of the electrodes. This position is subsequently equated with the depth EEG data to delineate the seizure onset zone as accurately as possible.

Because of the high radiation dose accompanying CT studies, it is preferable to examine the postimplantation patient solely with MR imaging. A two-dimensional spin-echo sequence may provide a method by which to view the electrode bundle and its contact points with limited susceptibility artifacts (5). However, if the intracerebral electrodes follow a curved trajectory, they may not be optimally captured in one section. Three-dimensional MR imaging with multiplanar reformatting provides an optimal way to show the electrode bundles throughout their course. Initially, 3-D MR images could only be obtained by using a gradient-echo sequence. However, when used with steel electrodes, this technique caused extensive susceptibility artifacts, making it impossible to locate the contact points. To overcome this obstacle, Duckwiler et al (6) used intracerebral electrodes that consisted of 79% platinum and a 21% alloy of rhodium and ruthenium. The disadvantage of using these electrodes is that they are more expensive than those made of stainless steel.

Three-dimensional fast spin-echo scans are inherently less susceptible to artifacts caused by metal implants. The $T2^*$ effect is reduced owing to the presence of refocusing 180° pulses following the 90° pulse. A T1-weighted sequence is preferred for demonstration of the anatomy of the brain; therefore, a T1-weighted fast spin-echo sequence was developed.

The proposed postimplantation MR imaging procedure (see data for patient 3 in the Table) shows the trajectory of the intracerebral electrodes as well as CT does. In addition, the high spatial and contrast resolution of MR imaging results in optimal visibility of the electrodes in relation to anatomic structures. The short echo time in this study, the large bandwidth, and the use of an appropriate direction of the phase-encoding gradient enabled us to identify the contact points on these MR images. This has not been possible with CT. If coronal reconstructions of axial 3-D sections are made, the clearest view of the contact points is obtained by using a phase-encoding gradient in the anteroposterior direction. The susceptibility artifacts associated with the direction of the frequency-encoding gradient will then be visible in the left-to-right direction. Sagittally reformatted images show the electrode contact points best if a left-to-right phase-encoding gradient is used.

Although the contact points on the intracerebral electrodes are well seen without deformation of surrounding tissues, the subdural electrode contact points remain difficult to distinguish from cerebrospinal fluid on the sequences described above. This problem may be overcome by using visually assisted contouring

of the electrode bundle on the 2-D reformatted images with 3-D reformatting of the brain and the electrodes.

One important point that remains to be addressed is the matter of the local increase in susceptibility artifacts at the contact points. The phantom study confirmed that the local areas of susceptibility artifacts coincided with the contact points. No paint or other materials were used at the site of the contact points. To study the possible susceptibility of the coating itself, a separate electrode with the coating removed was scanned over a longer distance. No difference in susceptibility artifacts was noted between coated and noncoated electrodes. To assess the configuration of the electrode bundle, a radiograph was made. A microscopic view showed the coating to be radiolucent and to appear as black dots. At the level of the contact points, the number of dots was reduced (Fig 1C), presumably because of a tighter twist of the electrode bundle, which resulted in a slight reduction of the diameter of the bundle (this was confirmed by a large-scale model made of electricity wires). This region was then associated with a different susceptibility. The change in susceptibility resulted in a local increase in dephasing and a larger susceptibility artifact. This finding may well prove to be of relevance in looking at MR-compatible guidewires during invasive MR procedures.

The overall result of the described scanning procedure is a reformatted scan with high spatial and high contrast resolution that provides satisfactory demarcation of the contact points of electrodes without significant distortion of surrounding brain tissue. The sequence has been applied successfully in two additional patients.

References

1. Van Veelen CWM, Debets RMC, Van Huffelen AC, et al. Combined use of subdural and intracerebral electrodes in preoperative evaluation of epilepsy. *Neurosurgery* 1990;26:93–101
2. Gerritsen FA, Van Veelen CWM, Mali WPTM, et al. Some requirements for and experience with covira algorithms for registration and segmentation. In: Beolchi L, Kuhn MH, eds. *Medical Imaging: Analysis of Multimodality 2D/3D Images.* Amsterdam, the Netherlands: IOS Press; 1995;19:4–28
3. Brooks ML, O'Connor MJ, Sperling MR, Mayer DP. Magnetic resonance imaging in localization of EEG depth electrodes for seizure monitoring. *Epilepsia* 1992;33:888–891
4. Zhang J, Wilson CL, Levesque MF, Behnke E, Lufkin RB. Temperature changes in nickel-chromium intracranial depth electrodes during MR scanning. *AJNR Am J Neuroradiol* 1993;14: 497–500
5. Spencer SS, So NK, Engel J Jr, Williamson PD, Levesque MF, Spencer DD. Depth electrodes. In: Engel J Jr, ed. *Surgical Treatment of the Epilepsies.* 2nd ed. New York, NY: Raven Press; 1993: 359–376
6. Duckwiler GR, Levesque M, Wilson CL, Behnke E, Babb TL, Lufkin R. Imaging of MR-compatible intracerebral depth electrodes. *AJNR Am J Neuroradiol* 1990;11:353–354